Original Article

MOLECULAR METABOLISM

Antiretroviral therapy potentiates high-fat diet induced obesity and glucose intolerance

Mark E. Pepin [1,2], Lindsey E. Padgett [3,4], Ruth E. McDowell [3,4], Ashley R. Burg [3,4], Manoja K. Brahma [1], Cassie Holleman [5], Teayoun Kim [5], David Crossman [6], Olaf Kutsch [7], Hubert M. Tse [3,4], Adam R. Wende [1,], Kirk M. Habegger [3,5,*]**

ABSTRACT

Objective: Breakthroughs in HIV treatment, especially combination antiretroviral therapy (ART), have massively reduced AIDS-associated mortality. However, ART administration amplifies the risk of non-AIDS defining illnesses including obesity, diabetes, and cardiovascular disease, collectively known as metabolic syndrome. Initial reports suggest that ART-associated risk of metabolic syndrome correlates with socioeconomic status, a multifaceted finding that encompasses income, race, education, and diet. Therefore, determination of causal relationships is extremely challenging due to the complex interplay between viral infection, ART, and the many environmental factors.

Methods: In the current study, we employed a mouse model to specifically examine interactions between ART and diet that impacts energy balance and glucose metabolism. Previous studies have shown that high-fat feeding induces persistent low-grade systemic and adipose tissue inflammation contributing to insulin resistance and metabolic dysregulation via adipose-infiltrating macrophages. Studies herein test the hypothesis that ART potentiates the inflammatory effects of a high-fat diet (HFD). C57Bl/6J mice on a HFD or standard chow containing ART or vehicle, were subjected to functional metabolic testing, RNA-sequencing of epididymal white adipose tissue (eWAT), and array-based kinomic analysis of eWAT-infiltrating macrophages.

Results: ART-treated mice on a HFD displayed increased fat mass accumulation, impaired glucose tolerance, and potentiated insulin resistance. Gene set enrichment and kinomic array analyses revealed a pro-inflammatory transcriptional signature depicting granulocyte migration and activation.

Conclusion: The current study reveals a HFD-ART interaction that increases inflammatory transcriptional pathways and impairs glucose metabolism, energy balance, and metabolic dysfunction.

Keywords Antiretroviral therapy; Obesity; Glucose intolerance; Adipose tissue inflammation; Insulin resistance; Macrophage activation

1. INTRODUCTION

The acquired immunodeficiency syndrome (AIDS) was first identified in the early 1980s. At that time, 5-year survival rate was 3.4%, and patients faced a median survival of 12.5 months [1]. AIDS has since exploded into one of the worst epidemics of recorded history. In the last 40 years, world-wide prevalence has exceeded 35 million, more than half of which are women and children, with over 2 million new cases emerging each year. Insights into the pathogenesis of AIDS as an infection has led to the development of both public health preventive measures and long-term medical therapies. The underlying cause of AIDS is the RNA retrovirus human immunodeficiency virus (HIV), which targets CD4+ T cells and macrophages [2]. HIV integrates into the human genome, creating a persistent infection that requires life-long medical management [3].

The advent of antiretroviral therapy (ART) has significantly decreased mortality in HIV-infected patients [4,5]. However, long-term administration of ART medications is associated with a disproportionate rise

[1]Division of Molecular and Cellular Pathology, Department of Pathology, University of Alabama at Birmingham, Birmingham, AL, USA [2]Department of Biomedical Engineering, University of Alabama at Birmingham, Birmingham, AL, USA [3]Comprehensive Diabetes Center, University of Alabama at Birmingham, Birmingham, AL, USA [4]Department of Microbiology, University of Alabama at Birmingham, Birmingham, AL, USA [5]Division of Endocrinology, Diabetes, and Metabolism, Department of Medicine, University of Alabama at Birmingham, Birmingham, AL, USA [6]Department of Genetics, Heflin Center for Genomic Science, University of Alabama at Birmingham, Birmingham, AL, USA [7]Division of Infectious Diseases, Department of Medicine, University of Alabama at Birmingham, Birmingham, AL, USA

*Corresponding author. Department of Medicine — Endocrinology, Diabetes & Metabolism, University of Alabama at Birmingham, Birmingham, AL 35294, USA. E-mail: kirkhabegger@uabmc.edu (K.M. Habegger).

**Corresponding author. Department of Pathology — Division of Molecular & Cellular Pathology, University of Alabama at Birmingham, Birmingham, AL 35294, USA. E-mail: adamwende@uabmc.edu (A.R. Wende).

Abbreviations: AIDS, acquired immunodeficiency syndrome; ART, antiretroviral therapy; ATM, adipose tissue macrophage; DIO, diet-induced obesity; eWAT, epididymal white adipose tissue; GTT, glucose tolerance test; SD, standard chow diet; HFD, high fat diet; HIV, human immunodeficiency virus; HOMA-IR, homeostatic model assessment of insulin resistance; ITT, insulin tolerance test; NAFLD, non-alcoholic fatty liver disease; NO, nitric oxide; NRTIs, nucleoside reverse-transcriptase inhibitors; PTK, protein tyrosine kinase; ROS, reactive oxygen species; STK, serine/threonine kinase; T2D, type-2 diabetes

Received March 2, 2018 • Revision received March 28, 2018 • Accepted April 2, 2018 • Available online 20 April 2018

https://doi.org/10.1016/j.molmet.2018.04.006

in non-AIDS-related mortality. Prolonged ART does not restore proper immune function, and patients often exhibit premature immunological aging, persistent immune hyper-activation, and chronic inflammation [6]. This is particularly troublesome given the decreased metabolic control in the HIV-1 patient population [7] are co-morbidities, including cardiovascular diseases [8], obesity [9], non-alcoholic fatty liver disease (NAFLD), and type-2 diabetes (T2D) [10,11]. Likewise, insulin resistance is observed in 35–63% of patients receiving ART, which greatly exceeds its prevalence in uninfected control populations [12–14].

There is growing interest in understanding metabolic syndrome in HIV-infected adults [15], yet the molecular mechanisms underlying metabolic syndrome in the context of HIV-1 infection under ART remain poorly understood. Thus, a deeper understanding of the complex interplay of genetics, immune responses, and therapeutic factors is needed to successfully develop clinical strategies against metabolic syndrome in HIV-1 patients.

Data herein illustrate that ART worsens HFD-induced metabolic derangements and exaggerates diet-induced adiposity. Combined transcriptomic and kinomic analyses of adipose tissue identified a diet-drug synergism that augments pro-inflammatory signaling within adipose tissue consistent with macrophage infiltration. These observations therefore support ongoing efforts to identify both novel therapeutic targets and modifiable clinical risks to improve the health and wellness of HIV-infected individuals.

2. RESEARCH DESIGN AND METHODS

2.1. Animal model

A cohort of 6-week-old, C57Bl/6J mice were obtained from the Jackson Laboratory. Mice were maintained on standard chow (4.7 kcal %, #7917, Envigo, Indianapolis, IN) until 8 weeks of age, then given *ad libitum* access to standard chow or high fat diet (HFD, 58.0 kcal% fat, #D12331 Research Diets, New Brunswick, NJ) for 12 weeks. Mice were group-housed (5/cage) on a 12:12-h light–dark cycle at 25 ± 1 °C and constant humidity with free access to food and water except as noted. Antiretroviral Therapy (ART/Atripla; Efavirenz, Emtricidabine, and Tenofovir disoproxil fumarate) was administered mixed within the diet such that dietary intake supplied ART doses equivalent to that of HIV patients (1100 mg/d or 14.67 mg/kg/d). All studies were approved by and performed according to the guidelines of the University of Alabama at Birmingham Institutional Animal Care and Use Committee.

2.2. Energy balance and body composition

Food intake and body weight were measured weekly. Body composition was assessed via non-invasive nuclear magnetic resonance spectroscopy (EchoMRI; Echo Medical Systems, Houston, TX) at the UAB Nutrition Obesity Research Center Small Animal Phenotyping Core.

2.3. Glucose and insulin tolerance tests

Glucose and insulin tolerance tests (GTT, ITT) performed by intraperitoneal (i.p.) injection of glucose (1.5 (chow-fed) or 2 g/kg (HF-fed), 20% wt/vol D-glucose [Sigma] in 0.9% wt/vol saline) or insulin (0.75 unit/kg in 0.9% wt/vol saline) to 6-hour fasted mice. Blood glucose was determined using TheraSense Freestyle Glucometer.

2.4. Tissue isolation

Following 12 weeks of diet/ART administration, mice were fasted for 2 h (starting at 0800). Mice were briefly sedated with pentobarbital prior to decapitation. Trunk blood was collected, and epididymal white adipose tissues (eWAT) were harvested and stored at −80 °C until analysis. A portion of the eWAT was processed for adipose tissue macrophage isolation as described below.

2.5. Adipose-infiltrating macrophage isolation

eWat tissue was minced, homogenized, and placed on a 40 μM strainer to obtain a single-cell suspension. Adipose macrophages were isolated by positive selection using biotinylated anti-F4/80 (eBioscience), streptavidin-conjugated magnetic beads (Miltenyi Biotec), and a LS magnetic column (Miltenyi Biotec) according to the manufacturer's protocol. Column-bound cells were then washed, counted, and frozen as a cell pellet for kinomic analysis.

2.6. Kinomic analysis

The isoMultiplex *In Vitro* Kinase Assay platform uses a high-throughput peptide microarray system to analyze 144 tyrosine phosphorylatable peptides and 144 serine/threonine phosphorylatable peptides that have been imprinted and immobilized in a 3-D format to examine kinase activity of tissue lysate. Protein lysate of eWAT-isolated macrophages were analyzed as previously described [16,17]. Briefly, isolated macrophage lysate was pooled yielding 3 pooled samples for each group to supply sufficient protein. Lysates were quantified and normalized using a dual standard BCA assay and dsDNA concentration then loaded at protein equivalents of 15 μg/well (Protein Tyrosine Kinase, PTK) or 2 μg/well (Serine/Threonine Kinase, STK) onto the PamChips for analysis using the PamStation12 instrument and software (Bionavigator software version 5.1, PamGene International, 's-Hertogenbosch, The Netherlands). Raw fluorescence images were imported to BioNavigator for quantitative analysis. The first step in quantification required background normalization, allowing for fluorescence quantification at 10, 20, 50, 100, and 200 ms exposure. A slope-exposure value was then Log_2-transformed for differential quantitation. To generate upstream kinase predictions, a *post hoc* unpaired t-test was then completed using Log_2-transformed relative intensities via Kinexus Phosphonet (www.phosphonet.ca), from which a "Normalized Kinase Statistic" was generated to rank and score putative kinase activity. Lastly, a Specificity Score was also computed to estimate the uniqueness of an identified kinase from associated phosphopeptides.

2.7. RNA sequencing analysis

Sequencing data have been deposited within the Gene Expression Omnibus repository (https://www.ncbi.nlm.nih.gov/geo/query/acc.cgi?acc=GSE110035). Tissue RNA was isolated using the RNeasy Lipid Mini-Kit according to the manufacturer's instructions (Qiagen, Valencia, CA). High-throughput RNA sequencing was performed at the Heflin Genomics Core at the University of Alabama at Birmingham. Alignment of reads to the mm10 genome was accomplished using STAR [18], raw counts generated using Samtools [19], and differential gene expression performed using DESeq2 [20] (1.18.1) within the R (3.4.2) statistical computing environment. Due to the sample size ($n = 2$), dispersion estimates were first determined via maximum likelihood, assuming that genes of similar average expression strength possess similar dispersion, as previously described [20]. Gene-wise dispersion estimates were then shrunken according to the empirical Bayes approach, providing normalized count data for genes proportional to both the dispersion and sample size. Differential expression was determined from normalized read counts via log_2 (fold-change) using the Wald test followed by Bonferroni-adjusted *P*-value (i.e. *Q*-value) for each aligned and annotated gene. Statistical significance was

assessed via unpaired two-tailed Bonferroni-adjusted *P*-value (*Q*-value) < 0.05. Differentially expressed genes (DEGs) were assumed biologically significant when $|\text{Log}_2\text{FoldChange}| > 1$ with normalized count sum > 1.

2.8. Data visualization

Functional and network GSEA, along with curated literature-supported candidate upstream regulators, were performed using QIAGEN's Ingenuity Pathway Analysis (IPA®, QIAGEN Redwood City, www.qiagen/ingenuity) on RNA sequencing datasets (Fold-Change > 2, $P < 0.05$, FPKM > 2). Within this software, pathway analysis was done both on the individual datasets and as a combined 'comparison' analysis to determine overlapping enriched pathways. Heat map generation was performed using *pheatmap* package (1.0.8) within R, and VennPlex [21] was used to create the Venn diagrams and determine overlapping genes. CIBERSORT was utilized to assess for transcriptional enrichment of immunologic cell types [22].

2.9. Quantitative real-time PCR

RNA was isolated as described above. cDNA was synthesized by reverse transcription PCR using SuperScript III, DNase treatment and anti-RNase treatment (Invitrogen, Carlsbad, CA). Single gene qPCR was performed as previously described [23]. Data were normalized to housekeeping gene cyclophilin (*Ppia*), a complete list of primers and targets is provided in Supplementary Table S1.

2.10. Statistics

All data are represented as mean ± standard deviation unless otherwise indicated. Glucose disappearance rate (k_g) defined as (Δ blood glucose/minute). Statistical significance was determined using unpaired Student's *t*-tests or, where appropriate, one- and two-way analysis of variance (ANOVA) with multiple comparisons Tukey and Sidak post-test, respectively. Statistical analyses and data visualization were completed using GraphPad Prism version 7.0 for Macintosh (GraphPad Software, San Diego, CA) and R software, version 3.4.2 (R Foundation for Statistical Computing, Vienna, Austria). Statistical significance was assigned when $P < 0.05$ unless otherwise specified.

3. RESULTS

3.1. ART exacerbates diet-induced obesity

Increased rates of obesity, T2D, and cardiovascular disease observed in ART-treated individuals suggest that ART may induce metabolic dysregulation. However, any changes in these individuals will be impossible to segregate from the effects of HIV-infection prior to treatment. Thus, we set out to assess the effects of ART on energy balance and glucose metabolism in a rodent model of diet-induced obesity (DIO). Eight-week old C57Bl/6J mice were assigned to groups matched for body weight and fat mass then provided *ad libitum* access to high-fat diet (HFD) or standard chow diet (SD), with or without ART. Mice maintained on SD displayed a slight decrease in % body weight gain in the presence of ART (Figure 1A, C; time—drug interaction, $P = 0.003$) as well as a trend ($P = 0.058$) for decreased body weight gain (Figure 1E). Conversely, and consistent with clinical observations, DIO in HFD-fed mice was exaggerated in the presence of ART (Figure 1B, D; time—drug interaction, $P < 0.0001$) and was associated with a 29.5% increase in total body weight gain relative to the BW change in HFD-VEH (Figure 1F).

In chow-fed mice, ART reduction in body weight was associated with normal accumulation of fat mass (Figure 2A, B) and a slight reduction in lean mass accumulation (Figure 2C, D). HFD-fed mice on ART displayed a greater final (Figure 2E) and change in fat mass over the 12-week study (Figure 2F) that was associated with increased lean mass accrual (Figure 2G, H). In HFD-fed mice, ART was associated with increased food intake throughout the study (Supplementary Figure S1A) and an overall increase in cumulative and total food intake as compared to vehicle controls (Supplementary Figures S1B, C).

3.2. ART worsens diet-induced glucose dysregulation

Increased adiposity and glucose homeostasis are often inversely associated [24]. We therefore assessed glucose tolerance after 8 weeks of ART treatment to determine its effect on glucose regulation. Similar to its effects on obesity, ART stimulated a mild increase in the glucose tolerance of SD-fed mice as determined by reduced glucose excursion and area under the curve (AUC) analysis (Figure 3A). Conversely, HFD-ART mice displayed greater intolerance as determined by glucose excursion and AUC analysis as compared to the already glucose intolerant vehicle-HF-fed mice (Figure 3B). Furthermore, while SD-ART mice displayed a trend ($P = 0.054$) for increased insulin action as determined by glucose excursion and rate of disappearance (k_{g45}; Figure 3C) during i.p. ITT. In contrast, HFD-fed mice treated with ART exhibited a trend of decreased insulin action as compared to HFD-VEH mice (Figure 3D). Although fasting blood glucose of ART-treated mice was not different from vehicle-controls in either diet (Figure 3E), ART-treated, HFD-fed mice displayed exaggerated hyperinsulinemia as compared to the already hyperinsulinemic HFD-fed controls (Figure 3F). This hyperinsulinemia also drove an elevation in insulin resistance as determined by HOMA-IR (Figure 3G). Altogether these data suggest that ART synergistically disrupts glucose metabolism and energy balance in a diet-dependent manner.

3.3. ART potentiates diet-induced inflammatory transcriptomic changes in adipose tissue

To determine whether shifts in the transcriptional landscape underlie the physiologic decrements observed in HFD-ART feeding, we performed RNA sequencing of epididymal white adipose tissue (eWAT). Hierarchical clustering and heatmap visualization of the ART vs. VEH revealed a modest segregation between HFD and SD mice within both ART- and VEH-treated groups ($P < 0.05$, Figure 4A and Supplementary Table S2). Examination of the overlapping differentially expressed genes (DEGs) by ART in the SD- and HFD-fed mice (i.e. ART specific effects) elucidated only 199 genes of the total 1,089 DEGs (Figure 4B and Supplementary Tables S3—S5). To determine whether HFD-ART synergy adversely affects the metabolic transcriptional programming of eWAT, differentially-expressed genes were examined according to known association with GO-term pathway "Diabetes Mellitus Signaling in Adipocytes", identifying the following 9 genes (Figure 4C): *Adipoq*, *Ikbke*, *Fgfr2*, *Irs1*, *Irs2*, *Pik3cg*, *Pik3r5*, *Prkaa2*, and *Prkcd*. Furthermore, the most robustly differentially expressed gene by Log_2(Fold-Change) in HFD-ART vs. HFD-VEH was G-protein coupled receptor 50 (*Gpr50*) (35.5-fold, $Q < 0.001$), induction of which has been previously implicated in the dysregulation of glucose homeostasis (Figure 4D) [25].

To examine gene networks likely responsible for the observed metabolic transcriptional reprogramming, GO Term (i.e. 'Canonical') pathway enrichment was used to rank regulatory pathways by both statistical significance and percent enrichment. This analysis uncovered pathways linked to macrophage-phagocytosis (phagocytosis in macrophages and phagosome formation), -activation/signaling (LXR/RXR activation, pattern recognition receptors, nitric oxide (NO) and reactive oxygen species (ROS) signaling in macrophages, IL-8

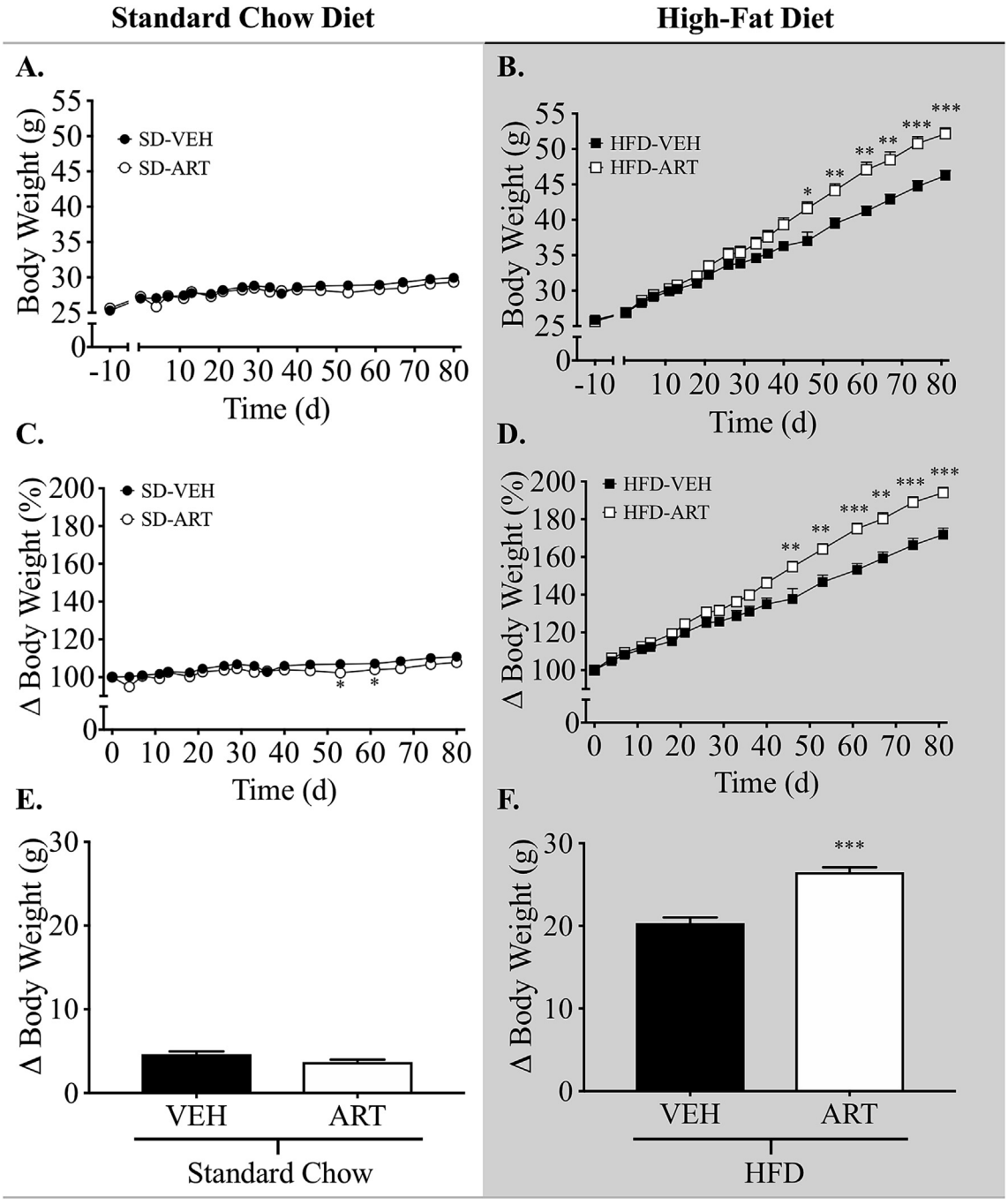

Figure 1: Effect of HFD and ART on Body Weight. Body weight was measured weekly in mice fed (A) normal chow or (B) high-fat diet (HFD) to examine differences in ART- versus vehicle-treated (VEH) mice ($n = 10$). Change in body weight relative to weight at t = 0 for (C) normal chow-fed or (D) HFD-fed mice. Change in body weight after the 80-day treatment period for (E) normal chow-fed and (F) HFD-fed mice, relative to starting body weight. All statistical comparisons were using 2-way ANOVA, reporting group mean (±S.E.). *$P < 0.05$, **$P < 0.01$, ***$P < 0.001$.

signaling, and GM-CSF signaling), and cytoskeleton rearrangement (actin cytoskeleton signaling) (Figure 4E).

Examining the genes responsible for enriching the top 5 pathways revealed a sub-group of genes that were assigned to many of the top pathways, most notably *Sema4d*, *Pgf*, *Plxnc1*, *Fes*, *Sdcbp*, and *Fgfr2*. Furthermore, the majority of genes responsible for driving pathway enrichment were increased in HFD-ART relative to HFD-VEH (Figure 5). Together, these observations provide evidence that an immunologic cell population shift could be driving the differential gene expression.

3.4. ART-stimulated immune cell flux

To determine which infiltrating immunologic cell types, if any, were likely responsible for the pathway enrichment, the RNA sequencing data were inspected further using CIBERSORT [26], a supervised machine learning model for cellular deconvolution. We combined this model with a transcriptional signature matrix of isolated immune cell types as developed by Chen et al. [27]. Unsupervised (unbiased) hierarchical clustering of the resulting enrichment matrix revealed that the effect of ART in SD-fed mice produced trivial effects on the immune

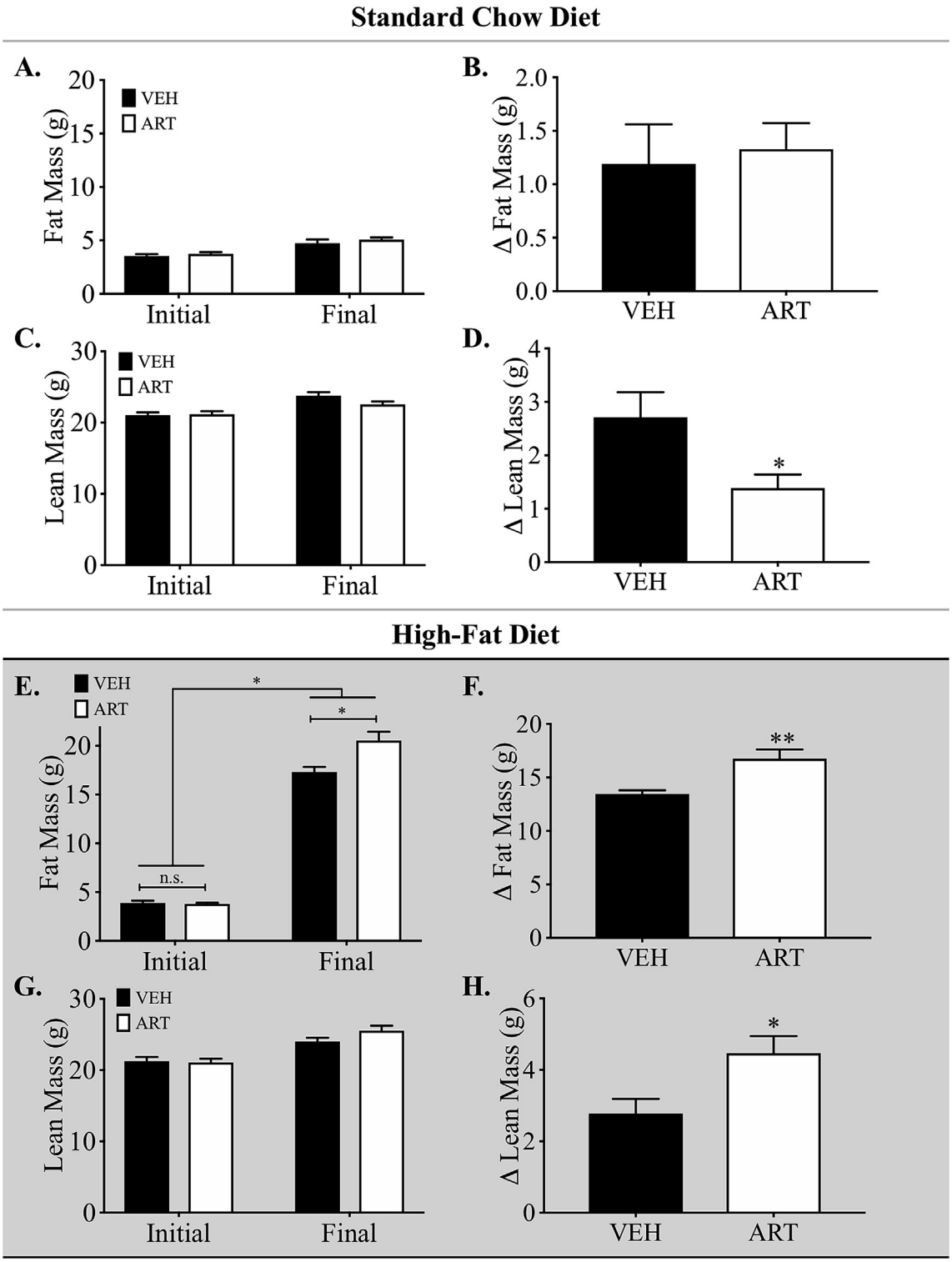

Figure 2: Effect of HFD and ART on Body Composition. Body composition was measured in mice given standard chow diet with or without ART, with (A) fat mass (grams) before and after 80-day experiment, (B) change in fat mass from the duration of the experiment, (C) lean mass, and (D) change in lean mass throughout the experiment ($n = 10$). Body composition was measured in mice given high-fat diet with or without ART, with (E) fat mass (grams) before and after 80-day experiment, (F) change in fat mass from the duration of the experiment, (G) lean mass, and (H) change in lean mass throughout the experiment. All statistical comparisons were using 2-way ANOVA, reporting group mean (±S.E.). $^{*}P < 0.05$, $^{**}P < 0.01$.

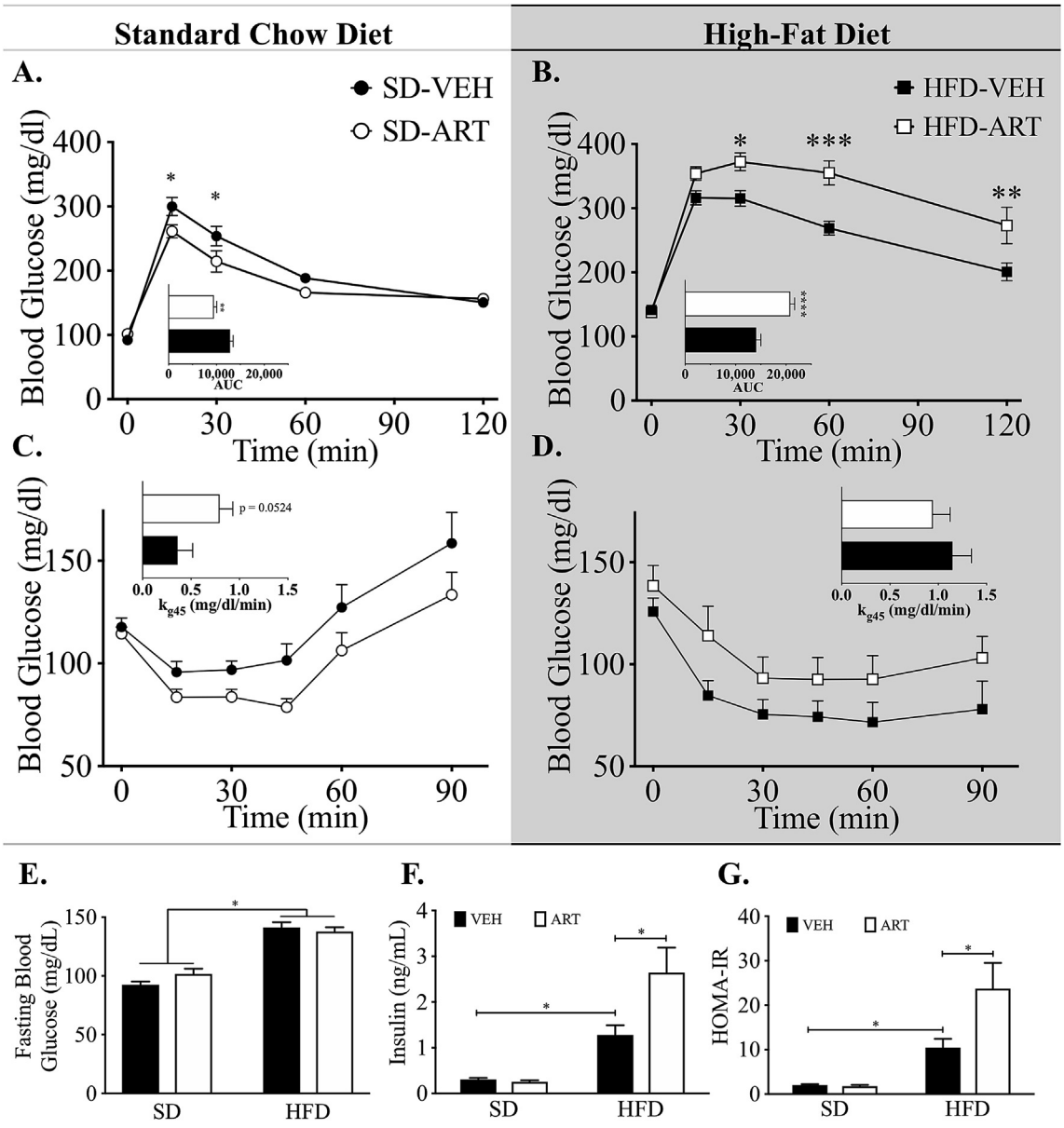

Figure 3: Effect of HFD and ART on Glucose Homeostasis. Intraperitoneal (i.p.) glucose tolerance testing (GTT) was performed on mice given (A) standard chow diet with/without ART ($n = 8$), or (B) high-fat diet with/without ART ($n = 10$). I.p. insulin tolerance testing (ITT) was performed on mice given (C) standard chow diet with/without ART ($n = 8$), or (D) high-fat diet with/without ART ($n = 10$). (E) Four-hour fasting blood glucose measurements were taken across all 4 experimental groups at 12-weeks. (F) ELISA-based methods were used to measure circulating insulin levels in all 4 groups at 12-week time point. (G) Homeostatic model assessment of insulin resistance (HOMA-IR) was calculated for all 4 experimental groups at the 12-week time-point using the equation HOMA-IR = ([Glucose] × [Insulin])/405. All statistical comparisons were using 2-way ANOVA, reporting group mean (±S.E.). *$P < 0.05$, **$P < 0.01$, ***$P < 0.001$.

signature, whereas diet appeared to drive sample clustering (Figure 6A). Nevertheless, it was evident that, among the HF-fed mice, a sub-clustering existed between ART- and VEH-treated mice. This analysis therefore shows a predictive model capable of distinguishing HFD-ART from HFD-VEH groups based solely on their immune signature.

In order to determine the immune cell type(s) responsible for driving the group clustering, we then quantified the proportional enrichment of each isolated immune cell type (Figure 6B). This analysis elucidated an increased macrophage enrichment in HFD-VEH relative to SD-VEH mice (Figure 6B). Furthermore, while ART failed to increase macrophage signature in SD-fed mice, HFD-ART mice exhibited robustly increased macrophage expression beyond that of HF-feeding alone (Pearson's $\rho = 0.70$, $P < 0.01$) (Figure 6B). This observation was consistent with the gene set enrichment analysis, suggesting that eWAT-infiltrating macrophages are at-least partially responsible for differential gene expression in the HFD-ART vs. VEH-HFD comparison. We next looked to putative upstream regulators to determine whether known cytokines or signaling cascades could confirm the CIBERSORT-based immunologic enrichment analysis (Figure 6C). This analysis suggested activation and enrichment of established upstream regulators of M1 macrophage polarization (TNF-α, IL-6, and CSF2). Lastly, in order to authenticate this immunologic signature, we examined macrophage gene expression markers (Figure 6D), which exhibited an

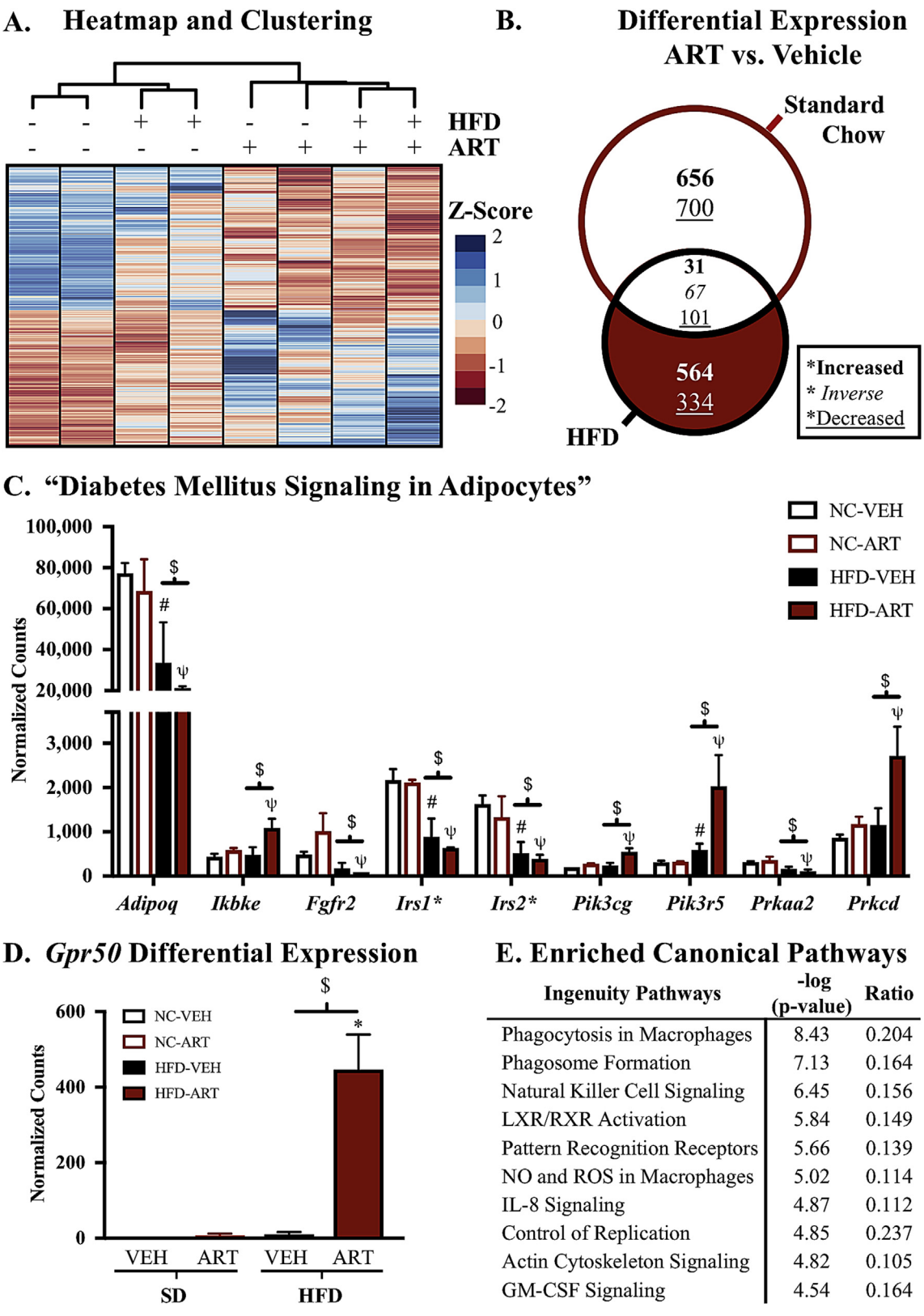

Ingenuity Pathways	-log (p-value)	Ratio
Phagocytosis in Macrophages	8.43	0.204
Phagosome Formation	7.13	0.164
Natural Killer Cell Signaling	6.45	0.156
LXR/RXR Activation	5.84	0.149
Pattern Recognition Receptors	5.66	0.139
NO and ROS in Macrophages	5.02	0.114
IL-8 Signaling	4.87	0.112
Control of Replication	4.85	0.237
Actin Cytoskeleton Signaling	4.82	0.105
GM-CSF Signaling	4.54	0.164

Figure 4: Dietary Differences in the Transcriptional Effect of ART in eWAT. (A) Hierarchical clustering and heatmap visualization of differential gene expression ($n = 2$) based on ART vs. VEH comparison ($P < 0.05$); complete gene list and fold-changes listed in Supplementary Table S2. (B) Venn Diagram of differentially-expressed genes by ART vs. Vehicle for the SD- or HFD-fed mice; complete gene list and fold-changes per sector listed in Supplementary Tables S3–S5. (C) Gene Set Enrichment Analysis was performed on the differentially expressed genes (DEGs) by ART vs. Vehicle comparison only in HFD ($P < 0.05$) to determine differential expression of HFD-ART vs. HFD-VEH ($P < 0.05$) was used to populate GO-Term Pathway "Diabetes Mellitus Signaling in Adipocytes". (D) Most robustly differentially-expressed gene and *validation using qPCR ($n = 6$). Top 10 GO Term Enriched Pathways to identify putative upstream regulators. $ Q < 0.05$ for HFD-ART vs. HFD-VEH; Ψ $Q < 0.05$ for HFD-ART vs. SD-VEH; #$Q < 0.05$ for HFD-VEH vs. SD-VEH.

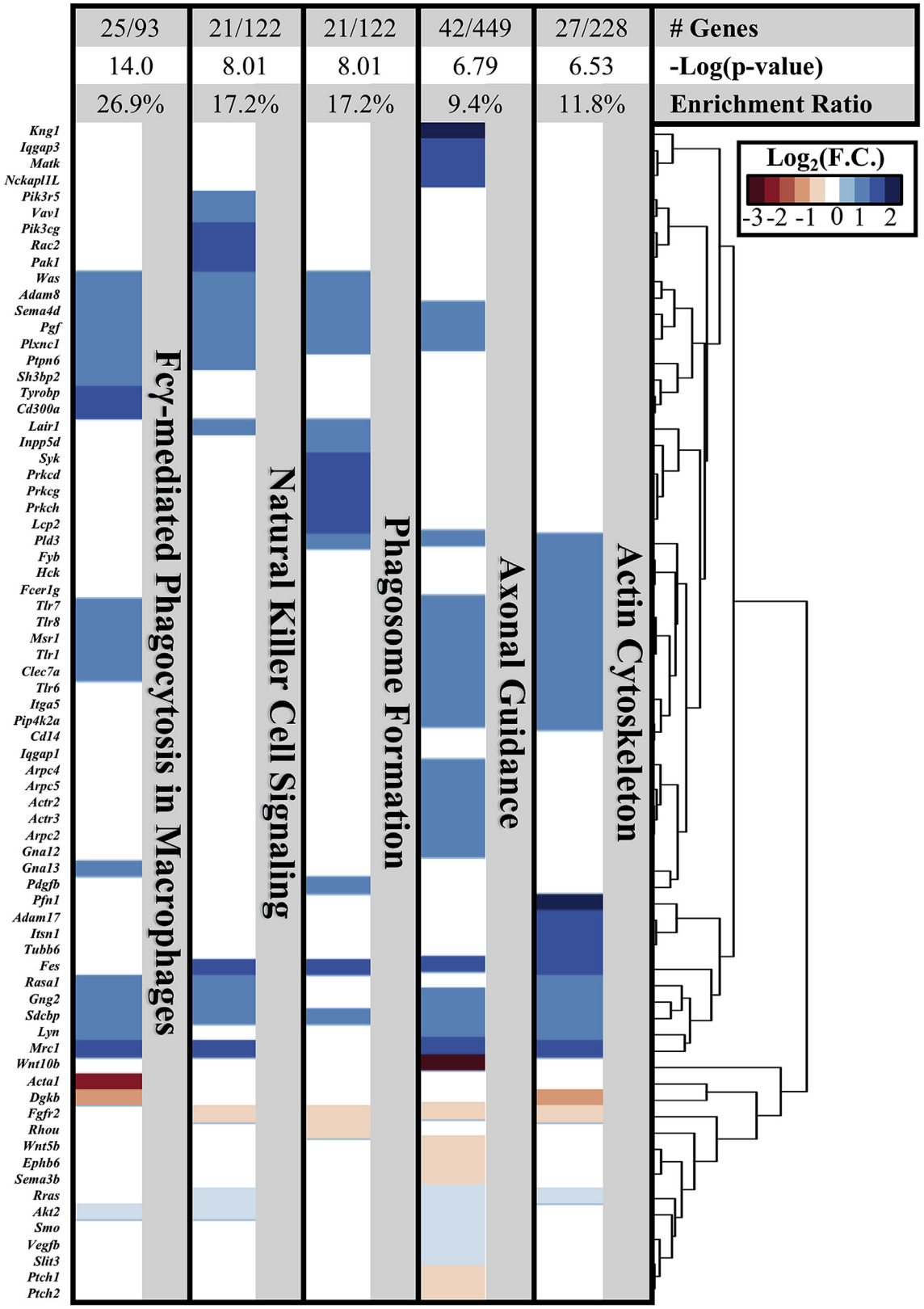

Figure 5: Hierarchical Pathway Enrichment Clustering. The genes responsible for populating the top 5 enriched pathways generated via Ingenuity Pathway Analysis (IPA) were clustered via Euclidean distance, with heatmap of Log_2(Fold-Change). Differential gene expression was assessed via RNA sequencing analysis ($n = 2$) and was considered significant at the $P < 0.05$ level for this visualization.

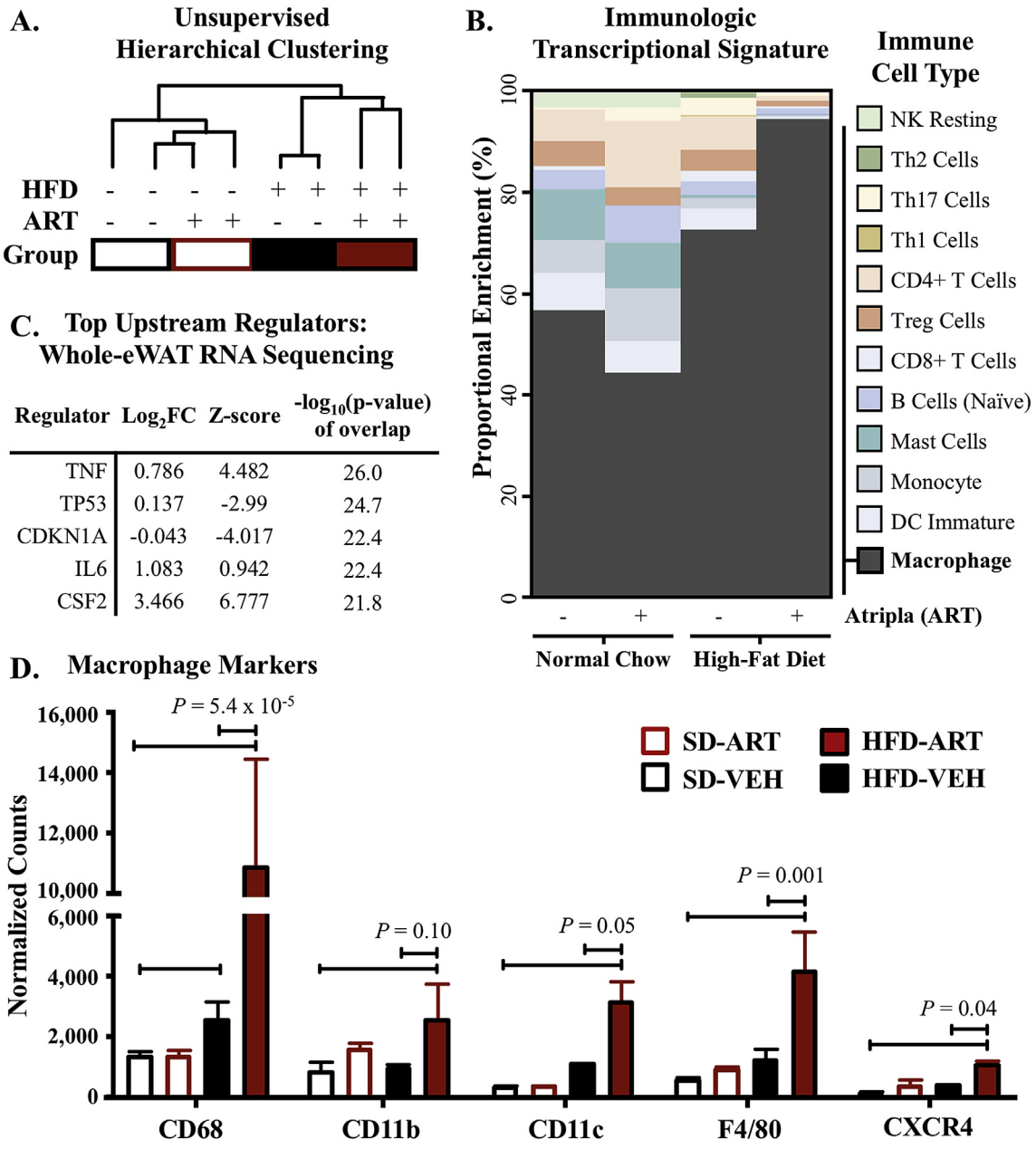

Figure 6: Whole-Tissue eWAT from HFD-ART Mice Possess a Transcriptional Fingerprint Consistent with Macrophage Enrichment. The CIBERSORT algorithm developed by Newman et al. [22] was used to estimate the proportional enrichment of sequenced isolated immune cells based on mRNA expression of whole-tissue eWAT ($n = 2$), using the signature expression matrix developed by Chen et al. [27]. (A) Unsupervised hierarchical clustering via Ward's minimum least squared method was used to determine the cell-type signature among eWAT samples by both Diet and Treatment. (B) Enrichment (%) of whole-tissue sequencing of eWAT under dietary and treatment conditions by isolated sequenced immunologic cell types, based on Pearson's correlation. (C) Pathway analysis to identify the top 5 upstream regulators to explain differential gene expression. (D) Mean gene expression (±S.D.) of common gene markers of macrophage infiltration and activation as determined by RNA-sequencing analysis of whole-tissue eWAT.

expression pattern that increased or trended upwards beyond that of HFD alone: CD68 (*Cd68*, 2.8-fold, $P = 5.4 \times 10^{-5}$), CD11b (*Itgam*, 1.5-fold, $P = 0.001$), CD11c (*Itgax*, 1.7-fold, $P = 0.054$), F4/80 (*Emr1*, 2.1-fold, $P = 0.001$), and CXCR4 (Cxcr4, 1.47-fold, $P = 0.035$). Gene markers of B lymphocytes (*Cd19*, *Ms4a1*, *Ptprc*, *Cd22*), T lymphocytes (*Cd3d*, *Cd3e*, *Cd3g*, *Cd4*, *Cd8a*), and neutrophils (Mpo, Ly6g5b, Ly6g6c and Ly6g6d) were not significantly changed in HFD-ART relative to HFD-VEH (Supplementary Figure S2). Altogether, these data suggest that the inflammatory eWAT transcriptional signature is likely due to the increased presence of adipocyte-infiltrating macrophages in the HFD-ART combination beyond that of HFD alone.

3.5. Kinomic analysis of isolated eWAT macrophages

Kinomic analysis of the eWAT infiltrating macrophages was conducted to predict upstream kinase activity and to identify putative intracellular regulators underlying the inflammatory signals and metabolic derangements. Interrogation of protein tyrosine kinase (PTK) activity suggested suppression of BMX non-receptor tyrosine kinase (encoded by *Bmx*), insulin receptor (encoded by *Insr*), and protein kinase C delta (encoded by *Prkcd*) in ART-treated HF-fed mice as compared to vehicle, HFD-fed controls (Figure 7A). This predicted kinase activity is consistent with the whole-eWAT transcriptional metabolic pattern noted previously. Most notably, however, was that Serine/Threonine

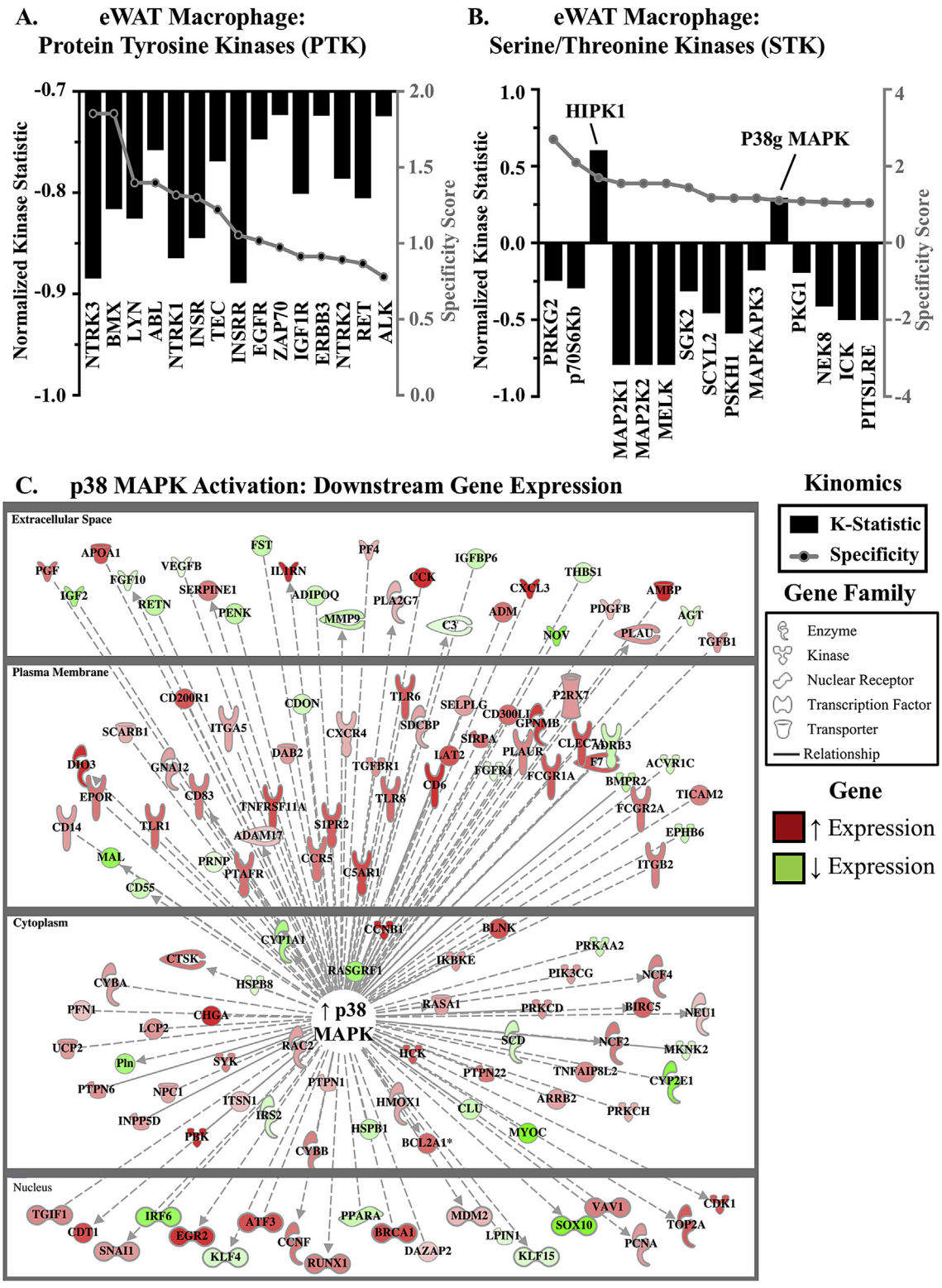

Figure 7: Regulatory Upstream Kinase Activity in ART-Diet Interaction. Kinomics-based analysis of putative upstream (A) Protein Tyrosine Kinase (PTK) and (B) Serine/Threonine Kinase (STK) activity, with kinases ranked according to both specificity score and k-statistic ($n = 3$). (C) $p38^{MAPK}$ nodal regulation via IPA® curation of differentially-expressed genes in HFD-ART vs. HFD-VEH ($P < 0.05$).

Kinase analysis revealed increased activity of $p38^{MAPK}$ and HIPK1(Figure 7B), both of which are central to macrophage M1 polarization and activation [28,29]. Lastly, we used a combined analysis comparing kinomic and transcriptomic signatures to determine if $p38^{MAPK}$ signaling was likely controlling and/or controlled by transcriptional changes (Figure 7C). We noted that, among the genes with known connection to $p38^{MAPK}$ signaling, many are involved in both macrophage activation (*Tlr1*, *Cd14*, *Cxcr4*, *Ccr5*, etc.) and metabolic activity (*Ppara*, *Klf4*, *Klf15*, *Igf2*, *Adipoq*, etc.). HIPK1 was also examined for overlapping gene interactions but lacked comparable enrichment (data not shown). Altogether, these data suggest that ART exacerbates HFD-induced macrophage infiltration and activation via $p38^{MAPK}$ activation.

4. DISCUSSION

Prior generations of protease inhibitors and thymidine-analogue nucleoside reverse-transcriptase inhibitors (NRTIs) were associated with lipodystrophy and impaired glucose uptake [12–14]. Newer therapeutics with lower side-effect profiles such as Atripla, have replaced these earlier interventions and abrogated much of the lipodystrophy observed in this population. However, the use of these next generation ARTs is accompanied by obesity, NAFLD, and elevated T2D risk [10,30,31]. Although clinically reported, the underlying mechanism(s) for these metabolic abnormalities remains unknown. In this study, we utilized a DIO rodent model (i.e. high fat fed C57Bl/6J mice) to investigate the physiology and molecular signals altered during ART treatment. The use of this model allows us to eliminate confounding factors associated with HIV infection to more specifically test the interaction of ART and diet. We identified transcriptional signatures of increased adipose tissue inflammation associated with exacerbated glucose intolerance and accelerated DIO in HFD-ART mice. We further investigated the kinomic regulation of adipose-resident macrophages and observed markers of inflammation and impaired insulin signaling following ART treatment.

We found that ART-induced fat mass accumulation and glycemic dysregulation surpasses HFD alone. Lean body mass also increased in HFD-ART beyond that of HFD alone, a finding that is particularly intriguing given the concomitant disruptions in glucose handling; increases in skeletal muscle would be expected to improve glucose tolerance even in the context of insulin insensitivity. Importantly, however, ART-impairment of glucose homeostasis and insulin resistance was restricted to HF-fed mice. This finding is consistent with the Veterans Aging Cohort Study, in which reverse transcriptase inhibitor-based HIV treatment profoundly increased the risk ratio of diabetes associated with increasing BMI [32]. The ART treatment utilized in the current study is a combination of efavirenz, emtricidabine, and tenofovir disoproxil fumarate. Used by almost a third of HIV-patients taking ART, the combination of efavirenz, emtricidabine, and tenofovir disoproxil fumarate is a common first-line therapeutic, but the combinatorial effects of this treatment on metabolic dysregulation has not been characterized [33]. Individually, efavirenz-based treatment is associated with a 21% insulin resistance prevalence, although this risk was reduced in patients treated with NRTIs rather than protease inhibitors [34], suggesting that efavirenz *per se*, may not be the driving factor. Emtricidabine treatment has not been associated with insulin resistance and importantly, emtricidabine and tenofovir fail to impair insulin resistance in healthy individuals [35]. Overall these reports, along with our current findings, suggest that a complex interaction between the combined components of ART treatment and HFD-feeding impairs regulation of energy balance and glucose metabolism. Recent findings suggest that ART-treated women display greater insulin sensitivity as compared to otherwise matched male patients, despite greater baseline risk factors [36]. Of note, our studies were conducted in male mice and thus we were unable to assess sex-associated differences, but our future studies will address sex-dependent ART effects. Such studies may require the use of thermoneutral animal housing, as prior studies examining sexual dimorphisms in metabolic response emphasize its importance in experimental design [37]. Importantly, our mouse model can be exploited, via depletion antibodies or genetic knockout strategies, to perform mechanistic studies to further examine the interplay of ART treatment and HFD on obesity and glucose metabolism in the absence of CD4 T cells, similar to patients with HIV.

Chronic, low-grade inflammatory hyper-activation has been established as a contributor to insulin resistance, obesity, and overall metabolic dysregulation [38]. This complex and systemic response involves macrophage infiltration into adipose tissue as well as the inappropriate production of inflammatory cytokines and chemokines such as IL-6, IL-1β, CCL2, and TNF-α [39]. In lean mice and humans, macrophages constitute around 5% of the cells in the adipose tissue, are dispersed throughout the tissue, and exhibit limited inflammatory properties [40–42]. However, during obesity, ATMs increase 10-fold and make up 50% of all adipose tissue cells [40]. Moreover, these ATMs surround dead adipocytes forming crown-like structures with a pro-inflammatory phenotype that is directly associated with insulin resistance [41,42]. ATMs are recruited to the adipose tissue via chemokine signaling, induce transcriptional changes in insulin-dependent metabolic signaling, and contribute to obesity-associated T2D [43]. Consistent with a causal role in the disease, systemic suppression of inflammation in T2D patients improves glycemic control [44]. However, this system is poorly understood in the context of HIV-infected patients. In the current study, we found that, although ART alone was insufficient to induce transcriptomic changes consistent with macrophage infiltration and activation, it induced robust inflammatory changes consistent with macrophage infiltration and activation in HF-fed mice beyond that of HFD alone. This finding is especially germane to HIV serodiscordant couples where ART is utilized in uninfected individuals to prevent transmission [45]. While examining this drug–diet interaction was warranted in the absence of HIV infection, future studies are needed to determine the effects of this diet-drug synergy within an immunocompromised host.

Macrophages display significant plasticity and in response to environmental triggers can polarize to two broad subtypes; “classical” M1 macrophages and “alternatively-activated” M2 macrophages [46]. However, the M1 and M2 macrophage nomenclature has been refined to depict the cytokine or polarization condition to induce multiple phenotypes including M(IL-4), M(Ig), M(IL-10), M(IFN-γ), M(LPS), etc. [47]. Partly due to their plastic nature and different models of obesity, classification of M1 and M2 macrophages as being pro-inflammatory and anti-inflammatory in adipose tissue is not rigid. As opposed to the production of pro- and anti-inflammatory cytokine synthesis, it has been proposed that the phenotype of ATMs should be characterized by changes in lipid metabolism since fatty acids are the main trigger for metabolic activation of ATMs [48]. Our transcriptional data demonstrate an increase in pro-inflammatory macrophage infiltration in adipose tissue and display a M1-like phenotype as evidenced by the activation of the $p38^{MAPK}$ pathway and an increased transcription of pro-inflammatory effector molecules including TNF-α, IL-8, NO, and ROS synthesis. However, there is evidence that M2-like macrophages in the adipose tissue of obese individuals can produce pro-inflammatory cytokines [49]. These ATMs display a heterogeneous phenotype of both

M1- and M2-type macrophage markers, but more importantly, are associated with insulin resistance [50]. Thus, our future studies will involve additional characterization of macrophage phenotypes from C57BL/6 mice on a HFD-ART regimen and, importantly, to define their contribution to insulin resistance and obesity. Likewise, although current studies have focused on eWAT inflammation, it is likely that similar defects are occurring other metabolic tissues (i.e. other adipose depots, liver, hypothalamus, and skeletal muscle).

In our search for a candidate regulator of the differential effects of ART in a diet-dependent manner, we found the "melatonin-related" G-protein coupled receptor 50 (*Gpr50*) as most robustly induced by RNA-sequencing and qPCR. Despite its structural similarity with the melatonin receptor family, *Gpr50* does not bind to melatonin. Instead, it has been shown to regulate whole-body energy and temperature homeostasis via its actions in the hypothalamus. Likewise, *Gpr50*-deficient mice exhibit lower body mass on normal chow and are DIO resistant [25]. Moreover, *Gpr50* regulates adaptive thermogenesis in response to leptin signaling [51], and polymorphisms in this gene have also been associated with increased levels of circulating triglycerides and obesity [52]. It is currently unknown if *Gpr50* regulates adipose-tissue macrophage infiltration or inflammation. However, our data support that ART-fed mice display enhanced eWAT *Gpr50* expression associated with metabolic dysfunction. Thus, our future analyses will determine if *Gpr50* is an effective molecular target. Importantly, we will determine if *Gpr50*-dependent signaling has a role in adipose-tissue inflammation under conditions of ART treatment and DIO in mouse models and in translational studies with patients with HIV that have metabolic syndrome.

While the current study is a necessary first step in identifying the interaction between ART and diet, additional studies are warranted to provide both mechanistic and contextual insight into the complexities of long-term HIV treatment. We observed that a high-calorie diet enriched in fat is required for ART-induced metabolic defects, it remains unknown whether it is the effect of specific nutrients, or total caloric excess via hyperphagia underlying these complication's. To test the latter, future studies will make use of the hyperphagic *ob/ob* mouse as well as energy-restricted pair-feeding of C57Bl/6J mice [53]. Likewise, chronic ART-treatment of HIV-infected individuals is associated with marked changes in the gut flora [54], a key regulator of metabolic homeostasis [55] that could also be contributing to the observed effects. Lastly, studies should examine other tissues to characterize the system-wide metabolic responses regulated by other tissues, since adipose tissue is one of many metabolic organs.

Until more effective targeted therapies are developed to address ART-associated metabolic syndrome, food-intake modification via dietary counseling remains the most promising method of clinical intervention. The use of lipid-lowering drugs improves risk of metabolic complications, but their use in HIV patients is avoided due to the heightened toxicity risks in HIV patients and drug interactions with ART [56]. Short-term dietary interventions to reduce fat intake have successfully attenuated the dyslipidemia associated with ART [57], although metabolic sequelae have not yet been adequately studied. HIV-positive patients with lower socioeconomic status suffer from higher mortality rates, an observation that is particularly alarming considering the disproportionately high incidence of HIV seroconversion in this demographic [58].

5. CONCLUSIONS

Together, these analyses provide an extensive description of the functional metabolic and transcriptional changes induced during anti-retroviral therapy and high-fat feeding. Our studies demonstrate that ART synergizes with high-fat feeding to induce chronic inflammatory signaling. This escalation of diet-induced inflammation likely results from enhanced eWAT macrophage infiltration that contributes to metabolic syndrome. Therefore, while chronic ART treatment has dramatically extended lifespan for HIV-infected individuals, it is apparent that these therapeutics also alter susceptibility to diet-induced metabolic defects. Our observations identify several avenues for novel targeted therapy, but moreover we highlight the potential importance of dietary intervention as a clinical consideration to improve the life-long management of HIV-infected individuals.

AUTHOR CONTRIBUTIONS

MEP, LEP, REM, ARB, MKB, CH, TK, DC, HMT, ARW, and KMH collected and analyzed data. MEP, OK, HMT, ARW, and KMH wrote the manuscript. All authors reviewed/edited the manuscript. Dr. Kirk Habegger is the guarantor of this work and, as such, had full access to all the data in the study and takes responsibility for the integrity of the data and the accuracy of the data analysis.

FUNDING SOURCES

This work was supported by a UAB Center for Aids Research Pilot and Feasibility award (CFAR; NIH P30 AI027767; HMT), a UAB Diabetes Research Center Pilot and Feasibility award (DRC; NIH P30 DK079626; KMH), and an American Diabetes Association Career Development Award (7-12-CD-11; HMT). This work was also supported by the following NIH awards: NIDDK R01 DK099550 to HMT, NIDDK R01 DK112934 to KMH, and NHLBI R01 HL133011 to ARW.

Trainee support was provided by an NIH T32 award (HD071866; MEP) and NIH NIAID (5T32AI007051-35) Immunologic Diseases and Basic Immunology T32 training grant (ARB and LEP).

ACKNOWLEDGMENTS

We thank the UAB Research Computing Facility for use of the *Cheaha* compute cluster for all raw RNA sequencing genome alignments and annotation. We also thank Dr. Joshua Anderson and the UAB Kinomics core for completing the kinomics array.

CONFLICT OF INTEREST DISCLOSURES

The authors declare no conflict of interest.

APPENDIX A. SUPPLEMENTARY DATA

Supplementary data related to this article can be found at https://doi.org/10.1016/j.molmet.2018.04.006.

REFERENCES

[1] Lemp, G.F., Payne, S.F., Neal, D., Temelso, T., Rutherford, G.W., 1990. Survival trends for patients with AIDS. Journal of the American Medical Association 263(3):402–406.

[2] Walker, B.D., Chakrabarti, S., Moss, B., Paradis, T.J., Flynn, T., Durno, A.G., et al., 1987. HIV-specific cytotoxic T lymphocytes in seropositive individuals. Nature 328(6128):345–348.

[3] Buchow, H.D., Tschachler, E., Gallo, R.C., Reitz Jr., M., 1989. HIV-I replication requires an intact integrase reading frame. Haematology and Blood Transfusion 32:402–405.

[4] Survival after introduction of HAART in people with known duration of HIV-1 infection. The CASCADE Collaboration, 2000. Concerted action on SeroConversion to AIDS and death in Europe. Lancet 355(9210):1158–1159.

[5] Anti-HIV agents. Starting HAART and its effect on survival. TreatmentUpdate 14(1), 2002:3–5.

[6] Appay, V., Kelleher, A.D., 2016. Immune activation and immune aging in HIV infection. Current Opinion in HIV and AIDS 11(2):242–249.

[7] Calvo, M., Martinez, E., 2014. Update on metabolic issues in HIV patients. Current Opinion in HIV and AIDS 9(4):332–339.

[8] Shahbaz, S., Manicardi, M., Guaraldi, G., Raggi, P., 2015. Cardiovascular disease in human immunodeficiency virus infected patients: a true or perceived risk? World Journal of Cardiology 7(10):633–644.

[9] Freitas, P., Carvalho, D., Santos, A.C., Matos, M.J., Madureira, A.J., Marques, R., et al., 2012. Prevalence of obesity and its relationship to clinical lipodystrophy in HIV-infected adults on anti-retroviral therapy. Journal of Endocrinological Investigation 35(11):964–970.

[10] Medapalli, R.K., Parikh, C.R., Gordon, K., Brown, S.T., Butt, A.A., Gibert, C.L., et al., 2012. Comorbid diabetes and the risk of progressive chronic kidney disease in HIV-infected adults: data from the Veterans Aging Cohort Study. Journal of Acquired Immune Deficiency Syndromes 60(4):393–399.

[11] Kalra, S., Kalra, B., Agrawal, N., Unnikrishnan, A., 2011. Understanding diabetes in patients with HIV/AIDS. Diabetology & Metabolic Syndrome 3(1):2.

[12] Samaras, K., 2009. Prevalence and pathogenesis of diabetes mellitus in HIV-1 infection treated with combined antiretroviral therapy. Journal of Acquired Immune Deficiency Syndromes 50(5):499–505.

[13] Boufassa, F., Goujard, C., Viard, J.P., Carlier, R., Lefebvre, B., Yeni, P., et al., 2012. Immune deficiency could be an early risk factor for altered insulin sensitivity in antiretroviral-naive HIV-1-infected patients: the ANRS COPANA cohort. Antiviral Therapy 17(1):91–100.

[14] Arama, V., Tiliscan, C., Streinu-Cercel, A., Ion, D., Mihailescu, R., Munteanu, D., et al., 2013. Insulin resistance and adipokines serum levels in a caucasian cohort of HIV-positive patients undergoing antiretroviral therapy: a cross sectional study. BMC Endocrine Disorders 13:4.

[15] Willig, A.L., Overton, E.T., 2014. Metabolic consequences of HIV: pathogenic insights. Current HIV/AIDS Reports 11(1):35–44.

[16] Labots, M., Gotink, K.J., Dekker, H., Azijli, K., van der Mijn, J.C., Huijts, C.M., et al., 2016. Evaluation of a tyrosine kinase peptide microarray for tyrosine kinase inhibitor therapy selection in cancer. Experimental & Molecular Medicine 48(12):e279.

[17] Gilbert, A.N., Shevin, R.S., Anderson, J.C., Langford, C.P., Eustace, N., Gillespie, G.Y., et al., 2016. Generation of microtumors using 3D human biogel culture system and patient-derived glioblastoma cells for kinomic profiling and drug response testing. Journal of Visualized Experiments (112).

[18] Dobin, A., Davis, C.A., Schlesinger, F., Drenkow, J., Zaleski, C., Jha, S., et al., 2013. STAR: ultrafast universal RNA-seq aligner. Bioinformatics 29(1):15–21.

[19] Li, H., Handsaker, B., Wysoker, A., Fennell, T., Ruan, J., Homer, N., et al., 2009. The sequence alignment/map format and SAMtools. Bioinformatics 25(16):2078–2079.

[20] Love, M.I., Huber, W., Anders, S., 2014. Moderated estimation of fold change and dispersion for RNA-seq data with DESeq2. Genome Biology 15(12):550.

[21] Cai, H., Chen, H., Yi, T., Daimon, C.M., Boyle, J.P., Peers, C., et al., 2013. VennPlex–a novel Venn diagram program for comparing and visualizing datasets with differentially regulated datapoints. PLoS One 8(1):e53388.

[22] Newman, A.M., Liu, C.L., Green, M.R., Gentles, A.J., Feng, W., Xu, Y., et al., 2015. Robust enumeration of cell subsets from tissue expression profiles. Nature Methods 12(5):453–457.

[23] Habegger, K.M., Stemmer, K., Cheng, C., Muller, T.D., Heppner, K.M., Ottaway, N., et al., 2013. Fibroblast growth factor 21 mediates specific glucagon actions. Diabetes 62(5):1453–1463.

[24] Ford, E.S., Williamson, D.F., Liu, S., 1997. Weight change and diabetes incidence: findings from a national cohort of US adults. American Journal of Epidemiology 146(3):214–222.

[25] Ivanova, E.A., Bechtold, D.A., Dupre, S.M., Brennand, J., Barrett, P., Luckman, S.M., et al., 2008. Altered metabolism in the melatonin-related receptor (GPR50) knockout mouse. American Journal of Physiology. Endocrinology and Metabolism 294(1):E176–E182.

[26] Chen, B., Khodadoust, M.S., Liu, C.L., Newman, A.M., Alizadeh, A.A., 2018. Profiling tumor infiltrating immune cells with CIBERSORT. Methods in Molecular Biology 1711:243–259.

[27] Chen, Z., Huang, A., Sun, J., Jiang, T., Qin, F.X., Wu, A., et al., 2017. Inference of immune cell composition on the expression profiles of mouse tissue. Scientific Reports 7:40508.

[28] Chan, E.D., Riches, D.W., 2001. IFN-gamma + LPS induction of iNOS is modulated by ERK, JNK/SAPK, and p38(mapk) in a mouse macrophage cell line. American Journal of Physiology - Cell Physiology 280(3):C441–C450.

[29] Rao, K.M., 2001. MAP kinase activation in macrophages. Journal of Leukocyte Biology 69(1):3–10.

[30] Crum-Cianflone, N., Tejidor, R., Medina, S., Barahona, I., Ganesan, A., 2008. Obesity among patients with HIV: the latest epidemic. AIDS Patient Care and STDs 22(12):925–930.

[31] Friis-Moller, N., Sabin, C.A., Weber, R., d'Arminio Monforte, A., El-Sadr, W.M., Reiss, P., et al., 2003. Combination antiretroviral therapy and the risk of myocardial infarction. New England Journal of Medicine 349(21):1993–2003.

[32] Butt, A.A., McGinnis, K., Rodriguez-Barradas, M.C., Crystal, S., Simberkoff, M., Goetz, M.B., et al., 2009. HIV infection and the risk of diabetes mellitus. AIDS 23(10):1227–1234.

[33] Horberg, M.A., Klein, D.B., 2010. An update on the use of Atripla in the treatment of HIV in the United States. HIV/AIDS (Auckland, N.Z.) 2:135–140.

[34] Araujo, S., Banon, S., Machuca, I., Moreno, A., Perez-Elias, M.J., Casado, J.L., 2014. Prevalence of insulin resistance and risk of diabetes mellitus in HIV-infected patients receiving current antiretroviral drugs. European Journal of Endocrinology 171(5):545–554.

[35] Spinner, C.D., Kern, K.E., Zink, A., Wolf, E., Balogh, A., Noe, S., et al., 2016. Neither boosted elvitegravir nor darunavir with emtricitabine/tenofovir disoproxil fumarate increase insulin resistance in healthy volunteers: results from the STRIBILD-IR study. Antiviral Therapy 21(7):627–631.

[36] Koethe, J.R., Jenkins, C.A., Petucci, C., Culver, J., Shepherd, B.E., Sterling, T.R., 2016. Superior glucose tolerance and metabolomic profiles, independent of adiposity, in HIV-infected women compared with men on antiretroviral therapy. Medicine (Baltimore) 95(19):e3634.

[37] Giles, D.A., Moreno-Fernandez, M.E., Stankiewicz, T.E., Graspeuntner, S., Cappelletti, M., Wu, D., et al., 2017. Thermoneutral housing exacerbates nonalcoholic fatty liver disease in mice and allows for sex-independent disease modeling. Nature Medicine 23(7):829–838.

[38] Hotamisligil, G.S., 2017. Inflammation, metaflammation and immunometabolic disorders. Nature 542(7640):177–185.

[39] Gregor, M.F., Hotamisligil, G.S., 2011. Inflammatory mechanisms in obesity. Annual Review of Immunology 29:415–445.

[40] Weisberg, S.P., McCann, D., Desai, M., Rosenbaum, M., Leibel, R.L., Ferrante Jr., A.W., 2003. Obesity is associated with macrophage accumulation in adipose tissue. Journal of Clinical Investigation 112(12):1796–1808.

[41] Lumeng, C.N., Deyoung, S.M., Bodzin, J.L., Saltiel, A.R., 2007. Increased inflammatory properties of adipose tissue macrophages recruited during diet-induced obesity. Diabetes 56(1):16–23.

[42] Cinti, S., Mitchell, G., Barbatelli, G., Murano, I., Ceresi, E., Faloia, E., et al., 2005. Adipocyte death defines macrophage localization and function in adipose tissue of obese mice and humans. The Journal of Lipid Research 46(11):2347–2355.

[43] Stephens, J.M., Pekala, P.H., 1991. Transcriptional repression of the GLUT4 and C/EBP genes in 3T3-L1 adipocytes by tumor necrosis factor-alpha. Journal of Biological Chemistry 266(32):21839–21845.

[44] Davis, N.J., Crandall, J.P., Gajavelli, S., Berman, J.W., Tomuta, N., Wylie-Rosett, J., et al., 2011. Differential effects of low-carbohydrate and low-fat diets on inflammation and endothelial function in diabetes. Journal of Diabetic Complications 25(6):371–376.

[45] Heffron, R., Thomson, K., Celum, C., Haberer, J., Ngure, K., Mugo, N., et al., 2017. Fertility intentions, pregnancy, and use of PrEP and ART for safer conception among East African HIV serodiscordant couples. AIDS and Behavior.

[46] Espinoza-Jimenez, A., Peon, A.N., Terrazas, L.I., 2012. Alternatively activated macrophages in types 1 and 2 diabetes. Mediators of Inflammation 2012:815953.

[47] Murray, P.J., Allen, J.E., Biswas, S.K., Fisher, E.A., Gilroy, D.W., Goerdt, S., et al., 2014. Macrophage activation and polarization: nomenclature and experimental guidelines. Immunity 41(1):14–20.

[48] Kratz, M., Coats, B.R., Hisert, K.B., Hagman, D., Mutskov, V., Peris, E., et al., 2014. Metabolic dysfunction drives a mechanistically distinct proinflammatory phenotype in adipose tissue macrophages. Cell Metabolism 20(4):614–625.

[49] Zeyda, M., Farmer, D., Todoric, J., Aszmann, O., Speiser, M., Györi, G., et al., 2007. Human adipose tissue macrophages are of an anti-inflammatory phenotype but capable of excessive pro-inflammatory mediator production. International Journal of Obesity 31(9):1420–1428.

[50] Wentworth, J.M., Naselli, G., Brown, W.A., Doyle, L., Phipson, B., Smyth, G.K., et al., 2010. Pro-inflammatory CD11c+CD206+ adipose tissue macrophages are associated with insulin resistance in human obesity. Diabetes 59(7):1648–1656.

[51] Bechtold, D.A., Sidibe, A., Saer, B.R., Li, J., Hand, L.E., Ivanova, E.A., et al., 2012. A role for the melatonin-related receptor GPR50 in leptin signaling, adaptive thermogenesis, and torpor. Current Biology 22(1):70–77.

[52] Bhattacharyya, S., Luan, J., Challis, B., Keogh, J., Montague, C., Brennand, J., et al., 2006. Sequence variants in the melatonin-related receptor gene (GPR50) associate with circulating triglyceride and HDL levels. The Journal of Lipid Research 47(4):761–766.

[53] Ellacott, K.L., Morton, G.J., Woods, S.C., Tso, P., Schwartz, M.W., 2010. Assessment of feeding behavior in laboratory mice. Cell Metabolism 12(1):10–17.

[54] Zilberman-Schapira, G., Zmora, N., Itav, S., Bashiardes, S., Elinav, H., Elinav, E., 2016. The gut microbiome in human immunodeficiency virus infection. BMC Medicine 14(1):83.

[55] Parekh, P.J., Balart, L.A., Johnson, D.A., 2015. The influence of the gut microbiome on obesity, metabolic syndrome and gastrointestinal disease. Clinical and Translational Gastroenterology 6:e91.

[56] Stein, J.H., 2016. Management of lipid levels and cardiovascular disease in HIV-infected individuals: just give them a statin? Topics in Antiviral Medicine 23(5):169–173.

[57] Lazzaretti, R.K., Kuhmmer, R., Sprinz, E., Polanczyk, C.A., Ribeiro, J.P., 2012. Dietary intervention prevents dyslipidemia associated with highly active antiretroviral therapy in human immunodeficiency virus type 1-infected individuals: a randomized trial. Journal of the American College of Cardiology 59(11):979–988.

[58] Cunningham, W.E., Hays, R.D., Duan, N., Andersen, R., Nakazono, T.T., Bozzette, S.A., et al., 2005. The effect of socioeconomic status on the survival of people receiving care for HIV infection in the United States. Journal of Health Care for the Poor and Underserved 16(4):655–676.

